Korean J. Chem. Eng., **21**(1), 48-58 (2004)

Flow Direction When Fan Shaped Geometry is Applied in Gas-Assisted Injection Molding: 1. Flow Model Theory and its Criteria for Predicting Flow Directions

Kwang-Hee Lim†

Department of Chemical Engineering, Daegu University, Kyungsan, Kyungbuk 712-714, Korea
(*Received 3 April 2003 • accepted 10 December 2003*)

Abstract−In part 1 of this paper a qualitative analytical method to predict the preferred gas flow direction in gas-assisted injection molding (GAIM), which involves flow through panel-areas of various fan-shaped geometries, and the criteria to apply the method were presented with appropriate assumptions. Then the definition of a resistance to initial velocity was proposed as a rule of thumb, by which the gas directions of GAIM were predicted under various fan-shaped geometries. Upon performing the simulation on them with commercial software (MOLDFLOW), we compared the ratio of simulated gas penetration lengths to both directions with the predicted ratio of resistances as well as the predicted direction of the gas flow in GAIM using the suggested rule of thumb herein presented. The predictions with the suggested rule of thumb were generally quite consistent with the results of simulation (MOLDFLOW). However the discrepancy between the ratio of gas penetration lengths and the ratio of resistances was observed to increase as the ratio $\left(\frac{\text{more}(H/R_0)(\text{one-side})}{\text{less}(H/R_0)(\text{the other-side})}\right)$ of the values of H/R_0 on both sides of fan-shaped cavities became bigger even though the suggested rule of thumb was assumed adequate to use until the case met the condition of $(H/R_0)^2 1/\tilde{\theta}^2 \ll 1$ and $(H/R_0)^2 \ll 1$. Nevertheless, the suggested rule of thumb was still effective as far as the direction of gas flow was concerned.

Key words: Fan-shaped Geometry, Direction of Gas Flow, Gas-Assisted Injection Molding, Gas Penetration Length, A Rule of Thumb, Simulation

INTRODUCTION

Most gas-assisted injection molded parts are by and large composed not only of a single section through which gas penetrates but also a nominal thin wall with gas channels traversing the parts. To design molds in such a way that the gas cores out all the channels or other thick sections without penetrating into the thin walls, one needs to predict the preferred direction of gas for a given geometry. Understanding of the rules governing the preferred direction of gas is important for trouble shooting during mold try outs as well as in design stages, which requires knowledge of the relations between resistance for the gas flow and process variables such as resin flow length, cross section area of cavity, melt temperature, and existence of short shot.

Primary and secondary gas penetration has been investigated in terms of gas-liquid interface and polymer melt front in GAIM by many researchers [Chen, 1995; Khayat et al., 1995; Chen et al., 1996a, b; Gao et al., 1997; Shen, 1997, 2001; Parvez et al., 2002]. However, their approaches cannot be regarded as a rule of thumb but are close to that of commercial software for GAIM in that numerical simulations are performed by the use of control volume/finite element method or boundary-element approach.

When there exists more than one unfilled region and these paths are competing for the direction of gas, it was believed that the gas preferred the direction of least resistance. In other words, during the injection stage the gas usually takes the path of least flow resistance to catch up with the melt front [Chen et al., 1996a, b]. Thus "gas goes to the direction of the least resistance" has been another common statement of GAIM experts. The rule of thumb on the direction of gas flow for GAIM has been investigated [Soh and Lim, 2002; Lim and Lee, 2003], and simulation packages have been used to verify the gas direction predicted by the rule of thumb. Soh and Lim [2002] suggested a definition of the resistance to velocity to predict the gas-preferred direction under the simplest geometry of two different pipes connected at one connection point. Lim and Lee [2003] proposed a criterion in the prediction of gas flow direction of GAIM as the resistance to the initial velocity of melt polymer at the nearest geometry to a gas injection point, in such a complex situation as runners or thick cavity of two square plates connected to cavities composed of four pipes with same length and different diameter connected in series and parallel. They showed why the comparison of the resistances to flow rates of resin often leads to a wrong prediction for the gas direction, while a comparison of proposed resistances generally leads to a valid prediction of gas-preferred direction.

Consider a simple panel part with a gas channel shown in Fig. 1 where a pipe is connected to a fan-shaped cavity with a vertex angle of 180° formed by two parallel plates and gas is injected at the point above where two cavities are connected. When gas enters the gate after the cavity is filled with resin as shown in Fig. 1, gas chooses either path 1 or path 2. This situation occurs in most panel shaped parts, including a typical example of a TV cabinet shown in Fig. 2.

To predict the gas path in the situation of Fig. 1, one needs to develop an equation to describe the pressure drop requirement for steady state flow through a fan-shaped cavity with a vertex angle of 180°

†To whom correspondence should be addressed.
E-mail: khlim@daegu.ac.kr

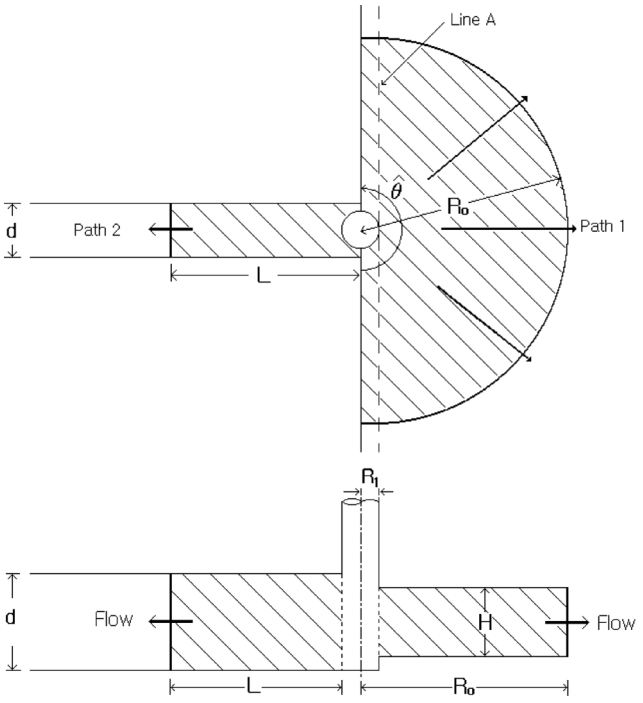

Fig. 1. The plan and side view of the flow of a molten polymer liquid in gas-assisted injection molding where a pipe is connected vertically to line A to a fan-shaped cavity with a vertex angle of 180º formed by two parallel plates and gas is injected at the point above where two cavities are connected.

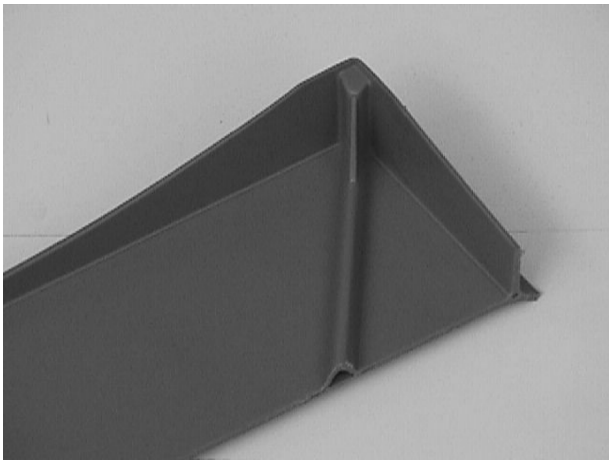

Fig. 2. A photograph of TV cabinet of which the molded panel part is a typical example of panel parts with gas channels traversing through them.

formed by two parallel plates. Eq. (1) describes the steady state flow of Newtonian liquids between infinite parallel flat plates neglecting end effects as shown in Fig. 3 [McCabe et al., 1986].

$$\Delta P = \frac{12\mu \overline{V} L}{a^2} \tag{1}$$

where

L : length of plate in direction of flow
a : distance between plates

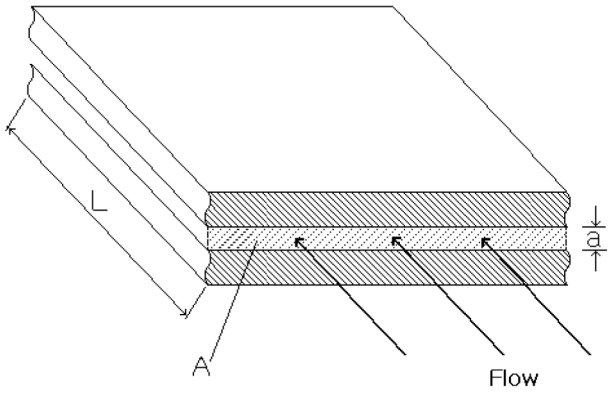

Fig. 3. The steady state flow of Newtonian liquids between infinite parallel plates

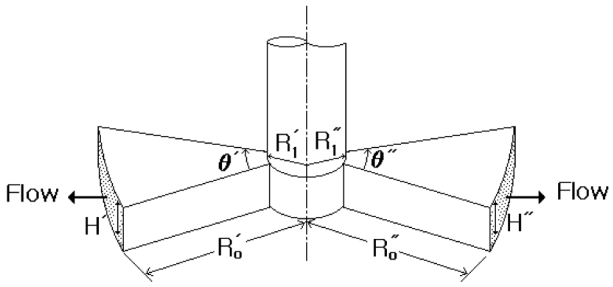

Fig. 4. The flow of a molten polymer liquid in gas assisted injection molding where two cavities formed by each pair of parallel fan-shaped plates are connected and gas is injected at the point above.

ΔP : pressure drop across the distance
$\overline{V}$: average velocity

However, Eq. (1) is not appropriate since it applies to a situation where the A side of Fig. 3 is under uniform pressure while the gas pressure is applied at one point, i.e., at the gate, not along line A in the situation of Fig. 1.

In part 1 of this paper a new equation is derived to describe the pressure drop requirement for a steady state flow through a general fan-shaped cavity formed by two parallel plates (Fig. 4), which has the same shape as or similar shape to the right hand side of Fig. 1. Then the definition of a resistance to initial velocity is proposed as a rule of thumb, by which the gas directions of GAIM are predicted under various fan-shaped geometries. Finally, upon performing a simulation on them with commercial software of MOLDFLOW (version of MPI 4.0) we compare the results of simulation performed with those of diagnosis on the gas flow in GAIM using the suggested rule of thumb presented herein to check the consistency of its predicted ratio of resistances as well as its predicted direction.

METHODS

1. Theory

For incompressible fluids, the continuity equation in cylindrical coordinates becomes:

$$\frac{1}{r}\frac{\partial}{\partial r}(rv_r) + \frac{\partial v_z}{\partial z} = 0 \tag{2}$$

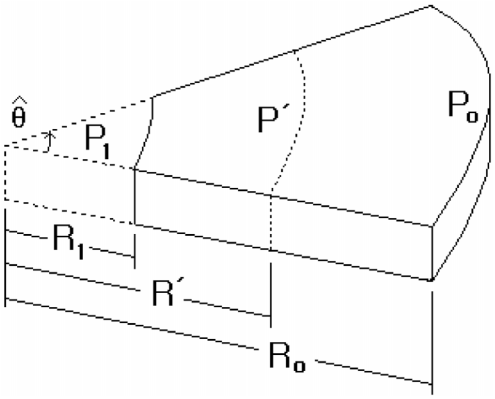

Fig. 5. The flow through between panel areas of fan-shaped geometry where a molten polymer liquid is fed into the mold at r=R_1 with the pressure of P_1 and is going out of the mold at r=R_0 with the pressure of P_0.

when v_θ is assumed to be zero velocity.

The momentum equation for a Newtonian fluid, neglecting gravity, becomes:

$$\rho\left(\frac{\partial v_r}{\partial t}+v_r\frac{\partial v_r}{\partial r}+v_z\frac{\partial v_r}{\partial z}\right)=-\frac{\partial P}{\partial r}+\mu\left[\frac{\partial}{\partial r}\left(\frac{1}{r}\frac{\partial}{\partial r}(rv_r)\right)+\frac{1}{r^2}\frac{\partial^2 v_r}{\partial\theta^2}+\frac{\partial^2 v_r}{\partial z^2}\right]$$

$$\rho\left(\frac{\partial v_z}{\partial t}+v_r\frac{\partial v_z}{\partial r}+v_z\frac{\partial v_z}{\partial z}\right)=-\frac{\partial P}{\partial z}+\mu\left[\frac{1}{r}\frac{\partial}{\partial r}\left(r\frac{\partial v_z}{\partial r}\right)+\frac{1}{r^2}\frac{\partial^2 v_z}{\partial\theta^2}+\frac{\partial^2 v_z}{\partial z^2}\right] \quad (3)$$

In order to compare the order of magnitude of each term of Eq. (2) & (3), one may make these equations dimensionless.

For the characteristic pressure of this geometry (Fig. 5), the force balance between r=R' (randomly chosen between r=R_1 and r=R_0) and r=R_0, can be approximated as below.

$$\hat{\theta}(R'hP'-R_0hP_0)=\frac{\hat{\theta}}{2}(R_0^2-R'^2)\mu\frac{\bar{v}_r}{h} \quad (4)$$

where $\hat{\theta}$ is the vertex angle of the fanshaped radial flow and $\bar{v}_r$ is not only average velocity between r=R' and r=R_0 but also characteristic velocity in r direction.

In Fig. 5, P_0 corresponds to the pressure of gas phase between leading melt phase front and the end of the mold with appropriate vent area in gas-assisted injection molding and is assumed to be negligible compared to P' so that P'>>$(R_0/R')P_0$.

Thus Eq. (4) can be reduced into:

$$\hat{\theta}R'hP'=\frac{\hat{\theta}}{2}(R_0^2-R'^2)\mu\frac{\bar{v}_r}{h} \quad (5)$$

Setting R' as $R_0/2$, P' becomes $3\mu\bar{v}_rR_0/4h^2$ which is $3\mu\bar{v}_rR_0/H^2$. Thus the characteristic pressure, $\bar{P}$, may be set as $\mu\bar{v}_rR_0/H^2$ to render dimensionless pressure, $\tilde{P}$, into $P/\bar{P}$ in this manner.

Further dimensionless variables are taken as:

$$\tilde{v}_r=\frac{v_r}{\bar{v}_r},\ \tilde{v}_z=\frac{v_z}{\bar{v}_z},\ \tilde{r}=\frac{r}{R_0},\ \tilde{z}=\frac{z}{H},\ \tilde{\theta}=\frac{\theta}{\hat{\theta}}\text{ and }\tilde{t}=\frac{t}{\hat{t}}$$

where $\hat{t}$ is chosen as $R_0/\bar{v}_r$ and $\bar{v}_z$ is chosen as $(H/R_0)\,\bar{v}_r$.

Then continuity and momentum equations are rendered into dimensionless form as below.

$$\frac{1}{\tilde{r}}\frac{\partial}{\partial\tilde{r}}(\tilde{r}\tilde{v}_r)+\frac{\partial\tilde{v}_z}{\partial\tilde{z}}=0 \quad (6)$$

$$\frac{\rho\bar{v}_rH}{\mu}\left(\frac{H}{R_0}\right)\left[\frac{\partial\tilde{v}_r}{\partial\tilde{t}}+\tilde{v}_r\frac{\partial\tilde{v}_r}{\partial\tilde{r}}+\tilde{v}_z\frac{\partial\tilde{v}_r}{\partial\tilde{z}}\right]$$
$$=-\frac{\partial\tilde{P}}{\partial\tilde{r}}+\frac{\partial^2\tilde{v}_r}{\partial\tilde{z}^2}+\left(\frac{H}{R_0}\right)^2\left(\frac{\partial}{\partial\tilde{r}}\left(\frac{1}{\tilde{r}}\frac{\partial}{\partial\tilde{r}}(\tilde{r}\tilde{v}_r)\right)\right)+\left(\frac{H}{R_0}\right)^2\frac{1}{\hat{\theta}^2}\left(\frac{1}{\tilde{r}^2}\frac{\partial^2\tilde{v}_r}{\partial\tilde{\theta}^2}\right) \quad (7)$$

$$\frac{\rho\bar{v}_rH}{\mu}\left(\frac{H}{R_0}\right)^3\left[\frac{\partial\tilde{v}_z}{\partial\tilde{t}}+\tilde{v}_r\frac{\partial\tilde{v}_z}{\partial\tilde{r}}+\tilde{v}_z\frac{\partial\tilde{v}_z}{\partial\tilde{z}}\right]$$
$$=-\frac{\partial\tilde{P}}{\partial\tilde{z}}+\left[\left(\frac{H}{R_0}\right)^4\left\{\frac{1}{\tilde{r}}\frac{\partial}{\partial\tilde{r}}\left(\tilde{r}\frac{\partial\tilde{v}_z}{\partial\tilde{r}}\right)+\frac{1}{\hat{\theta}^2}\frac{1}{\tilde{r}^2}\frac{\partial^2\tilde{v}_z}{\partial\tilde{\theta}^2}\right\}+\left(\frac{H}{R_0}\right)^2\frac{\partial\tilde{v}_z}{\partial\tilde{z}^2}\right] \quad (8)$$

When $(H/R_0)^2(1/\hat{\theta}^2)$<<1 and $(H/R_0)^2$ is the same order as or less than 0 (1), neglecting end effect on both sides in θ direction, the behavior of the flow between two fan-shaped plates in conventional injection molding may be considered as the part (i.e., $\hat{\theta}/2\pi$) of the radial flow between two entire round plates.

In addition, for and $\rho\bar{v}_r\,H/\mu(H/R_0)$<<1 and $(H/R_0)^2$<<1, Eq. (7) and Eq. (8) may be reduced into quasi-steady state equations:

$$0=-\frac{\partial\tilde{P}}{\partial\tilde{r}}+\frac{\partial^2\tilde{v}_r}{\partial\tilde{z}^2} \quad (9)$$

$$0=-\frac{\partial\tilde{P}}{\partial\tilde{z}} \quad (10)$$

$$\text{Thus }\frac{\partial P}{\partial r}=\mu\frac{\partial^2 v_r}{\partial z^2}=G(r) \quad (11)$$

with the boundary conditions of $v_r(r, z=h)=0$ and $v_r(r, z=-h)=0$.

The expression of v_r can be derived as

$$v_r(r,z)=\frac{h^2}{2\mu}G(r)\left(\frac{z^2}{h^2}-1\right) \quad (12)$$

Integrating Eq. (2) with z after one substitutes Eq. (12) into Eq. (2), one can derive such an expression as:

$$v_z(r,z)=-\frac{1}{r}\frac{\partial}{\partial r}(rG(r))\frac{h^2}{2\mu}\left(\frac{z^3}{3h^2}-z\right)+C_1(r)\ \text{ with boundary conditions: } v_z(r, z=h)=0 \text{ and } v_z(r, z=-h)=0.$$

Hence $v_z(r , z)$ becomes zero velocity due to $C_1(r)=0$ and $\partial/\partial r(rG(r))=0$.

Thus the pressure distribution becomes

$$P=\frac{P_1-P_0}{\ln\frac{R_1}{R_0}}\ln\frac{r}{R_0}+P_0 \quad (13)$$

where P_1 and P_0 is the pressure at r=R_1 and R_0 respectively.

The velocity profile is:

$$v_r(r,z)=\frac{h^2}{2\mu r}\frac{P_1-P_0}{\ln\frac{R_1}{R_0}}\left(\frac{z^2}{h^2}-1\right) \quad (14)$$

$$\text{when }\frac{\rho\bar{v}_rH}{\mu}\left(\frac{H}{R_0}\right)\ll1,\ \left(\frac{H}{R_0}\right)^2\frac{1}{\hat{\theta}^2}\ll1\text{ and }\left(\frac{H}{R_0}\right)^2\ll1 \quad (14\text{-}1)$$

Integrating $v_r(r, z)$ from Eq. (14) with z, the expression of melt phase flow rate (Q) of Eq. (15) is obtained as:

$$Q=\hat{\theta}rH\langle v_r\rangle=2\int_0^h v_r(r,z)\hat{\theta}r\,dz=\frac{2}{3}\frac{\hat{\theta}h^3}{\mu}\frac{P_1-P_0}{\ln\frac{R_0}{R_1}} \quad (15)$$

where $\langle v_r\rangle$: average velocity of melt phase flow

Eq. (15) may be rearranged as:

$$\Delta P_{fan\text{-}plates} = \frac{12\mu Q}{H^3\hat{\theta}}\ln\frac{R_0}{R_1} = \frac{12\mu r\langle V_r\rangle}{H^2}\ln\frac{R_0}{R_1} \quad (16)$$

2. Definition of Proposed Resistance

The definition of resistance may be develped and proposed to be r^* as a resistance to V^* of the initial velocity of melt polymer at the nearest geometry to a gas injection point while the resistance to flow rate was previously defined as $r^\#$ [Lim and Lee, 2003].

$$\Delta P = Qr^\# = V^* r^* \quad (17)$$

The proposed resistance of steady state flow of a Newtonian liquid under fan-shaped geometry may be rearranged, with the velocity at half of the distance of initial leading melt front, as below.

$$r^* = \frac{12\mu R_0}{H^2}\frac{R_0}{2}\ln\frac{R_0}{R_1} \quad (18)$$

The ratio of resistances to V^* of the velocity at half of the distance of initial leading melt front may be defined as the resistance of the geometry on L.H.S. divided by that on R.H.S. as below.

$$\frac{r^*}{r^{*\prime}} = \frac{H'^2 R_0}{H^2 R_0'}\frac{\ln\frac{R_0}{R_1}}{\ln\frac{R_0'}{R_1'}} \quad (19)$$

where a prime (') denotes the right hand side of two fan-shaped cavities.

3. Simulation

As shown in Fig. 4, two fan-shaped flows of a common pressure were considered with the same lengths of initial polymer shut-off to both of left and right directions to figure out the effect of vertex angle of fans as well as the thickness of fan-shaped cavity. Melt polymer was injected twice at different position of polymer injection nozzle in order to adjust the length of initial polymer shut-off the same to both directions. In addition, two fan-shaped flows of common pressure were simulated with different lengths of initial polymer shut-off as well as different thickness of cavities to both left and right directions. Finally, each effect of different vertex angle of fans, different length of initial polymer shut-off and different thickness of cavities of left and right directions, were independently investigated. The commercial software MOLDFLOW (version of MPI 4.0) was used to perform the simulations of which conditions are given as in Table 1.

The volume ratio of resin filling at polymer shut-off of each simulation was chosen between 85-95% to avoid blow-through at the stage of gas injection. In the modeling with MOLDFLOW adopting a control-volume-based finite element method (FEM) to track moving flow fronts, each node is supposed to formulate its control volume shared by the nodes of surrounding elements, which also applies to a gas injection node [Kennedy, 1995]. The control volumes are usually constructed by joining the centroid of each triangle element to the midpoints of the sides of that triangle element [Patankar, 1984]. When its neighboring elements are shown filled by melt resin or gas in the beginning of injection, its true leading front of a circle with the radius of polymer/gas nozzle, determined by its formulated control volume, exists between the gas injection node and its neighboring nodes. Thus, its apparent leading front is located farther than the true one, which generates a distance-gap between the apparent one and the true one, and stays still until its control volume occupied by polymer/gas nozzle is filled. The filling time is proportional to the formulated control volume of polymer/gas injection node occupied by the nozzle in the cavity. However, the time-varying behavior of the apparent leading front is available and is treated as an apparent or observed trajectory of polymer/gas leading front instead of the true one moving behind when a model is executed in the environment of MOLDFLOW. Since the radius of gas/polymer injection nozzle is the radius of true leading front in the beginning of injection and is in fact smaller by the distance-gap between the apparent one and the true one than the distance between the gas injection node and its neighboring nodes, apparent or observed trajectory may be considered as the true trajectory shifted up by the fore-mentioned distance-gap so that both trajectories may experience the same distance moved from their initial leading fronts. In apparent or observed trajectory, the apparent radius of initial leading front appeared to be the distance between the gas injection node and its neighboring nodes, which was adopted in this work as the apparent value of R_1 (i.e., the apparent radius of polymer or gas nozzle) for its convenience even though the true values of R_1 were smaller than the adopted values of R_1 due to the formulation of shared control volume of each node of the triangle element carrying polymer/gas injection node.

3-1. Simulations with the Same Length of Initial Polymer Shut Offs

Table 2 shows various geometrical conditions with the same length (43 mm) of initial polymer shut-off and the same mold (cavity) length (50 mm) on both directions for the simulations of GAIM. Six pairs of fan-shaped cavities were set in Figs. 6-1(a) to (c) and Figs. 6-2(a) to (c) in order to evaluate the effect of vertex angle of fan-shape with the same thickness of cavities.

Table 1. Simulation conditions of MOLDFLOW

Simulation ractor	Description
Resin filling	Short shot molding (85-95%)
Gas control	Volume control
Resin	PET(DP400)
Resin melt temperature	210 °C
Mold temperature	100 °C
Gas injection pressure	15 M pascal
Gas delay time	0.5 sec
Gas piston time	1 sec

Table 2. Various geometrical conditions of fan-shaped cavities (1)

Case	Position	Vertex angle	Thickness	R_1	R_0
Fig. 6-1	Left	(a) 30°, (b) 60°, (c) 90°	2 mm	9.4 mm	43 mm
	Right	(a) 90°, (b) 90°, (c) 90°	3 mm	9.4 mm	43 mm
Fig. 6-2	Left	(a) 30°, (b) 60°	3 mm	9.4 mm	43 mm
	Right	(a) 90°, (b) 90°	2 mm	9.4 mm	43 mm
Fig. 7	Left	30°	2 mm	9.4 mm	43 mm
	Right	90°	4 mm	9.4 mm	43 mm
Fig. 8	Left	30°	2 mm	9.4 mm	43 mm
	Right	90°	5 mm	9.4 mm	43 mm

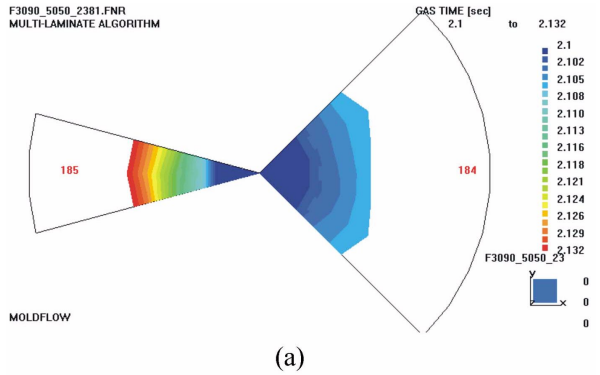

(a)

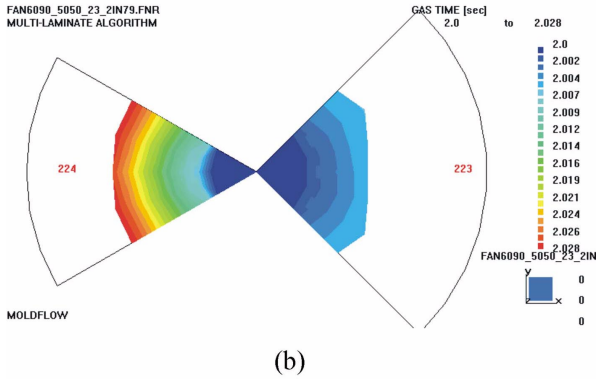

(b)

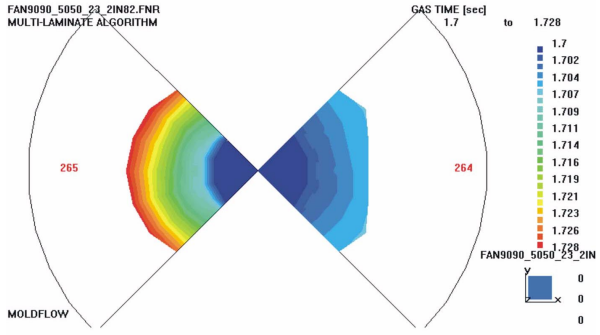

(c)

6-1

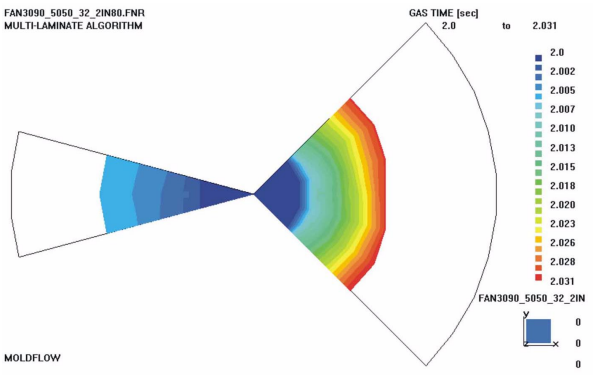

(a)

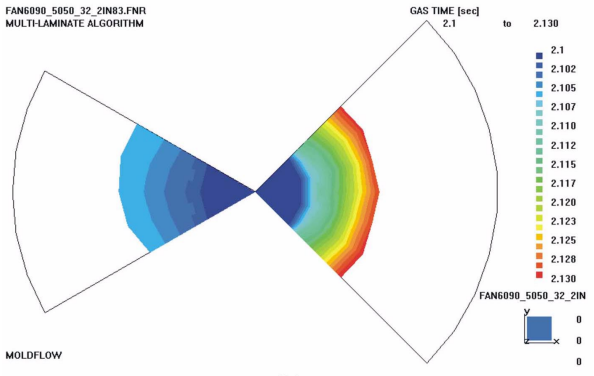

(b)

6-2

Fig. 6-1. Simulated gas penetration: (a) Left: $\hat{\theta}$=30º, H=2 mm; Right: $\hat{\theta}$=90º, H=3 mm; (b) Left: $\hat{\theta}$=60º, H=2 mm; Right: $\hat{\theta}$=90º, H=3 mm; (c) Left: $\hat{\theta}$=90º, H=2 mm; Right: $\hat{\theta}$=90º, H=3 mm. 6-2. Simulated gas penetration: (a) Left: $\hat{\theta}$=30º, H=3 mm; Right: $\hat{\theta}$=90º, H=2 mm; (b) Left: $\hat{\theta}$=60º, H=3 mm; Right: $\hat{\theta}$=90º, H=2 mm.

3-2. Simulations with the Same Vertex Angle of Fan Shapes

Table 3 shows various geometrical conditions with the same vertex angle (30º) of both fans on both sides for the simulations of GAIM.

3-3. Simulations with Various Vertex Angles of Fan Shapes, Various Lengths of Initial Polymer Shut-offs and Various Thicknesses of Cavities

Unlike the geometrical conditions in Tables 2 and 3, various geometrical conditions are given to each simulation of GAIM as in Table 4.

RESULTS AND DISCUSSION

1. Results with the Same Length of Initial Polymer Shut Offs

In Table 5 the results of simulation (SR) are compared with the output of rule of thumb (ratio of resistances) of GAIM with various geometrical conditions given in Table 2. SR denotes the ratio of simulated gas penetration length to both of right and left directions until either of right and left leading fronts reaches mold barrier first. Assuming that three nodes equally share the volume of the triangle element carrying polymer/gas injection node as a control volume, the true value of R_1 (i.e., the true radius of polymer or gas nozzle) would be approximated as the adopted values of R_1 multiplied by the factor of $1/\sqrt{3}$. The ratioes of resistance and the corrected ones in parenthesis (*i.e.*, those multiplied by the correction factor) were obtained as in Table 5, where the factor of $1/\sqrt{3}$ was considered to obtain the correction factor equivalent to the value of resistance with

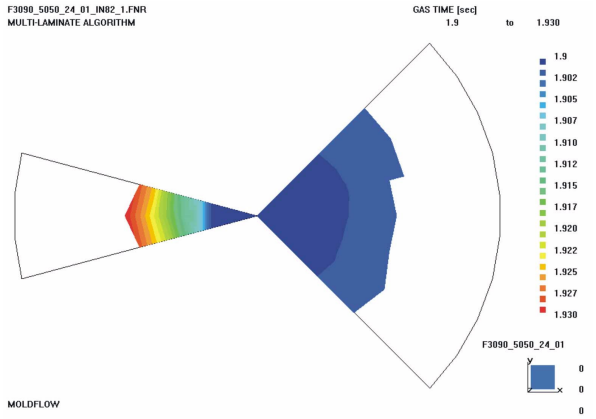

Fig. 7. Simulated gas penetration (Left: $\hat{\theta}$=30°, H=2 mm; Right: $\hat{\theta}$=90°, H=4 mm).

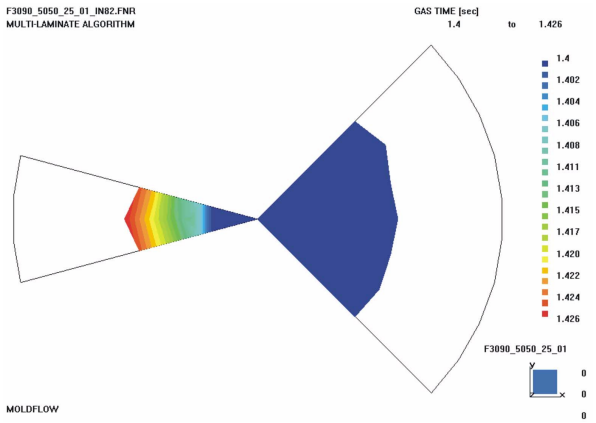

Fig. 8. Simulated gas penetration (Left: $\hat{\theta}$=30°, H=2 mm; Right: $\hat{\theta}$=90°, H=5 mm).

Table 3. Various geometrical conditions of fan-shaped cavities (2)

Case	Position	Vertex angle	Thickness	R_1	R_0
Fig. 9(a)	Left	30°	1 mm	3.1 mm	10 mm
	Right	30°	1.2 mm	4.8 mm	20 mm
Fig. 9(b)	Left	30°	1 mm	3.1 mm	10 mm
	Right	30°	1.5 mm	4.8 mm	20 mm
Fig. 9(c)	Left	30°	1 mm	3.1 mm	10 mm
	Right	30°	2 mm	4.8 mm	20 mm
Fig. 10(a)	Left	30°	1 mm	1.4 mm	10 mm
	Right	30°	1.1 mm	4.8 mm	40 mm
Fig. 10(b)	Left	30°	1 mm	1.4 mm	10 mm
	Right	30°	1.2 mm	4.8 mm	40 mm
Fig. 10(c)	Left	30°	1 mm	1.4 mm	10 mm
	Right	30°	2 mm	4.8 mm	40 mm
Fig. 10(d)	Left	30°	1 mm	1.4 mm	10 mm
	Right	30°	3 mm	4.8 mm	40 mm

true value of R_1 divided by that with adopted value of R_1.

It was observed that the effect of vertex angle of fan-shape with the same thickness of cavities was not remarkable as in Figs. 6-1(a) to (c) and Figs. 6-2(a) to (b). One may refer to both Eq. (14-1) and

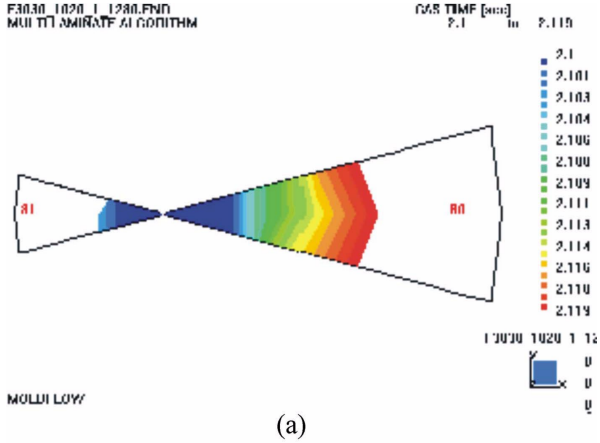

(a)

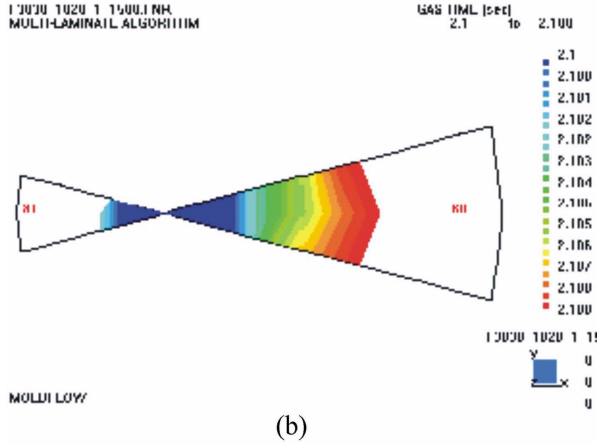

(b)

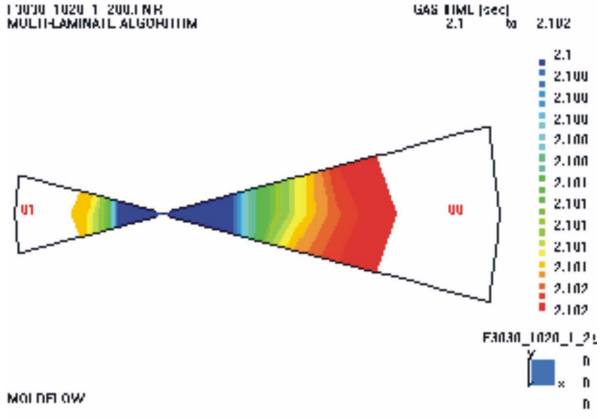

(c)

Fig. 9. Simulated gas penetration: (a) Left: R_0=10 mm, H=1 mm; Right: R_0=20 mm, H=1.2 mm; (b) Left: R_0=10 mm, H=1 mm; Right: R_0=20 mm, H=1.5 mm; (c) Left: R_0=10 mm, H=1 mm; Right: R_0=20 mm, H=2 mm.

Table 2 to check the validity of ratios of resistances given in Table 5. When $\tilde{r}$(i.e., r/R_0) may approaches zero under the condition of $R_1 \ll R_0$, neglected dimensionless inertial terms (e.g., $\tilde{v}_r(\partial\tilde{v}_r/\partial\tilde{r})$) may diverge around $r=R_1$ that for instance, even though dimensionless number of $\rho\tilde{v}_r H\mu/(H/R_0)$ satisfies the condition of Eq. (14-1), the order of magnitude of $\rho\tilde{v}_r H\mu/(H/R_0)\tilde{v}_r(\partial\tilde{v}_r/\partial\tilde{r})$ may become tantamount to that of pressure and viscous terms and the condition of negligible inertia may break down. Thus, the criteria to apply Eqs. (13),

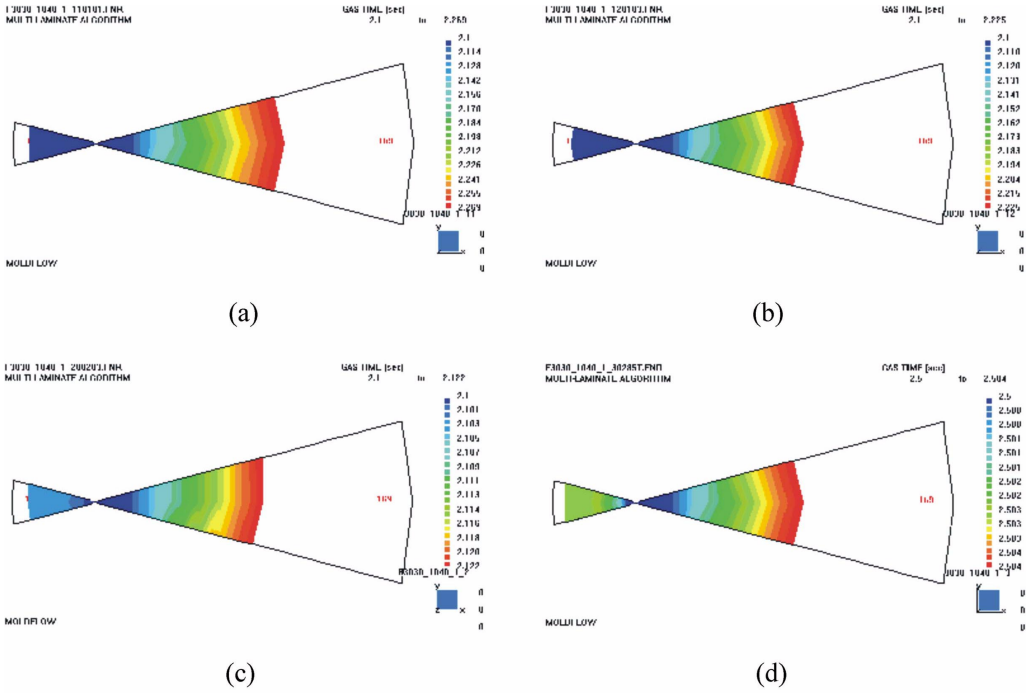

Fig. 10. Simulated gas penetration: (a) Left: R_0=10 mm, H=1 mm; Right: R_0=40 mm, H=1.1 mm; (b) Left: R_0=10 mm, H=1 mm; Right: R_0=40 mm, H=1.2 mm; (c) Left: R_0=10 mm, H=1 mm; Right: R_0=40 mm, H=2 mm; (d) Left: R_0=10 mm, H=1 mm; Right: R_0= 40 mm, H=3 mm.

Table 4. Various geometrical conditions of fan-shaped cavities (3)

Case	Position	Vertex angle	Thickness	R_1	R_0
Fig. 11(a)	Left	60°	1 mm	3.1 mm	10 mm
	Right	30°	1.1 mm	4.8 mm	20 mm
Fig. 11(b)	Left	60°	1 mm	3.1 mm	10 mm
	Right	30°	1.2 mm	4.8 mm	20 mm
Fig. 11(c)	Left	60°	1 mm	3.1 mm	10 mm
	Right	30°	1.5 mm	3.1 mm	20 mm
Fig. 12(a)	Left	60°	1 mm	3.1 mm	10 mm
	Right	60°	1.1 mm	3.1 mm	40 mm
Fig. 12(b)	Left	60°	1 mm	3.1 mm	10 mm
	Right	60°	1.2 mm	3.1 mm	40 mm
Fig. 12(c)	Left	60°	1 mm	3.1 mm	10 mm
	Right	60°	2 mm	3.1 mm	40 mm

Table 5. Comparison of the simulation-results to the output of rule of thumb (1)

Case	Gas directions	SR	Ratio of resistances	Correction factor
Fig. 6-1	Right	(a) 4.4	2.3 (2.3)	1
	Right	(b) 7.0	2.3 (2.3)	1
	Right	(c) 8.4	2.3 (2.3)	1
Fig. 6-2	Left	(a) 0.09	0.43(0.43)	1
	Left	(b) 0.11	0.43(0.43)	1
Fig. 7	Right	17.5	4.0 (4.0)	1
Fig. 8	Right	32.0	6.3 (6.3)	1

• SR denotes the ratio (right/left) of simulated gas penetration lengths to both of right and left directions until either of right and left leading fronts of melt-polymer reaches mold barrier first.
• The ratio (left/right) of resistance (the rule of thumb) was obtained from Eq. (19) and the value in the parenthesis is the corrected one (i.e., ratio of resistance multiplied by the correction factor.

(14) and (16) for the case of $R_1 \ll R_0$ needs to be established as below.

Making use of Eq. (14) and the expression of characteristic pressure (i.e., $\bar{P}=\mu\tilde{v}_r R_0/H^2$), $\tilde{v}_r(\partial\tilde{v}_r/\partial\tilde{r})$ at z=0 becomes $9/16(-1/\tilde{r})^3$ where $\tilde{r}$ is equal to r/R_0. Letting $\bar{v}_r$ be equal to $\langle v_r\rangle$ at $r=R_0/2$ so that $Q=\hat{\theta}(R_0/2)H\bar{v}_r$, the expression of $\bar{v}_r$ may be obtained from Eq. (15). Substituting this into $\rho\bar{v}_r H\mu/(H/R_0)$ and $\bar{v}_r(\partial\tilde{v}_r/\partial\tilde{r})$ at $\tilde{r}=R_1/R_0$ where the absolute value of $\bar{v}_r(\partial\tilde{v}_r/\partial\tilde{r})$ reaches its maximum, it becomes $\rho H^4/6\mu^2[(P_1-P_0)/(\ln(R_0/R_1)R_0^2)]$, where viscosity of 270 Pa sec is assumed, and $(-9/16)/(R_0/R_1)^3$, respectively. In addition, both the dimensionless pressure term (i.e., $-\partial\bar{P}/\partial\tilde{r}$) and dimensionless viscous term (i.e., $\partial^2\tilde{v}_r/\partial\tilde{z}^2$) from Eq. (7), may be evaluated at $\tilde{r}=R_1/R_0$ as $6(R_1/R_0)$. Thus the magnitudes of dimensionless terms of inertia (e.g., $\bar{v}_r(\partial\tilde{v}_r/\partial\tilde{r})$, pressure (i.e., $-\partial\bar{P}/\partial\tilde{r}$) and viscosity (i.e., $\partial^2\tilde{v}_r/\partial\tilde{z}^2$) are the same as the order of ten. Neglecting the inertia term may be valid even at $\tilde{r}=R_1/R_0$ as long as the magnitude of $\rho\bar{v}_r H\mu/(H/R_0)$ is very small. The dimensionless number of $\rho\bar{v}_r H\mu/(H/R_0)$ turned out to be the order of 10^{-3} to 10^{-4} so as to validate the application of the suggested rule of thumb.

It was noted that Eq. (19) may be adequate to use until the cases met the condition of $(H/R_0)^2(1/\hat{\theta}^2)\ll 1$ and $(H/R_0)^2\ll 1$. The discrepancy between SR and the ratio of resistances (i.e., discrepancy= |SR-Ratio of resistance/SR|) in Table 5 was observed to increase as the ratio (right/left) of the values of H/R_0 on both of right and left

Table 6. Comparison of the simulation-results to the output of rule of thumb (2)

Case	Gas directions	SR	Ratio of resistances	Correction factor
Fig. 9(a)	Left	0.5	0.59 (0.63)	1.06
Fig. 9(b)	Left	0.85	0.92 (0.98)	1.06
Fig. 9(c)	Right	1.83	1.63 (1.73)	1.06
Fig. 10(a)	Left	0.08	0.28 (0.29)	1.02
Fig. 10(b)	Left	0.08	0.33 (0.34)	1.02
Fig. 10(c)	Left	0.35	0.93 (0.95)	1.02
Fig. 10(d)	Right	1.38	2.08 (2.12)	1.02

• SR denotes the ratio (right/left) of simulated gas penetration lengths to both of right and left directions until either of right and left leading fronts of melt-polymer reaches mold barrier first.
• The ratio (left/right) of resistance (the rule of thumb) was obtained from Eq. (19) and the value in the parenthesis is the corrected one (i.e., ratio of resistance multiplied by the correction factor.

Table 7. Comparison of the simulation-results to the output of rule of thumb (3)

Case	Gas directions	SR	Ratio of resistances	Correction factor
Fig. 11(a)	Left	0.11	0.50 (0.53	1.06
Fig. 11(b)	Left	0.10	0.59 (0.63)	1.06
Fig. 11(c)	Left	0.40	0.71 (0.80)	1.13
Fig. 12(a)	Left	0.26	0.14 (0.17)	1.21
Fig. 12(b)	Left	0.26	0.16 (0.19)	1.21
Fig. 12(c)	Left	0.52	0.46 (0.56)	1.21

• SR denotes the ratio (right/left) of simulated gas penetration lengths to both of right and left directions until either of right and left leading fronts of melt-polymer reaches mold barrier first.
• The ratio (left/right) of resistance (the rule of thumb) was obtained from Eq. (19) and the value in the parenthesis is the corrected one (i.e., ratio of resistance multiplied by the correction factor.

hand sides of Fig. 4 became bigger, which may be attributed to not only the effective condition of the proposed flow model (i.e., $(H/R_0)^2(1/\hat{\theta}^2)\ll 1$ and $(H/R_0)^2\ll 1$) but also the actual phenomena excluded from the flow model that shear rate thinning property of pseudo-plastic fluid as well as melt resin flow of declining mass due to accumulated coated layer would accelerate the gas flow in a higher degree to the direction of R.H.S. or, in general, to the direction of less resistance according to Eq. (19). However, the suggested rule of thumb of Eq. (19) was still effective as in Table 5 as long as the direction of gas flow was concerned, when the direction of gas flow is defined as that of longer length of gas penetration between through right and left fan-shaped cavities until either of right and left leading melt-polymer fronts reaches mold barrier first, even though the discrepancy between SR and the ratio of resistance sometimes grows.

2. Results with the Same Vertex Angle of Fan Shapes

With various geometrical conditions given in Table 3 the results of simulation (SR) are compared with the output of rule of thumb (ratio of resistance) of GAIM as in Table 6. SR denotes the ratio of simulated gas penetration length to both of right and left directions until either of right and left leading fronts reaches mold barrier first. The ratioes of resistance and the corrected ones in parenthesis were treated in the same manner as in the previous section and obtained as in Table 6. The magnitudes of dimensionless terms of inertia (e.g., $\tilde{v}_r(\partial\tilde{v}_r/\partial\tilde{r})$ are the same order as or about ten times larger than those of pressure (i.e., $-\partial\tilde{P}/\partial\tilde{r}$) and viscosity (i.e., $\partial^2\tilde{v}_r/\partial\tilde{z}^2$). However neglecting the inertia term may be valid even at $r=R_1$ since the magnitudes of $\rho\bar{v}_r H\mu/(H/R_0)$, are so small as to be the order of 10^{-4}.

As in Table 6, it was showed that the predictions of suggested rule of thumb (Eq. (19)) were quite well matched by the simulation-results (the values of SR) of MOLDFLOW. However, in case of Figs. 10(a) and 10(b), the discrepancies between SR and the ratio of resistances (i.e., discrepancy=|SR-Ratio of resistance/SR|) were amplified. Thus, it was again confirmed that the discrepancy between SR and the ratio of resistances was observed to increase as in Table 6, by the same reasoning as in the previous section, as the ratio (left/right) of the values of H/R_0 on left and right sides became bigger. However, the direction of gas flow was always correct so that the rule of thumb of Eq. (19) might be still effective when the definition of direction of gas flow is used as previously defined.

3. Results with Various Vertex Angles of Fan Shapes, Various Lengths of Initial Polymer Shut-offs and Various Thicknesses of Cavities

In Table 7 the results of simulation (SR) are compared with the output of rule of thumb (ratio of resistance) of GAIM with various geometrical conditions given in Table 4. SR denotes the ratio of simulated gas penetration length to both of right and left directions until either of right and left leading fronts reaches the mold barrier first. The ratioes of resistance and the corrected ones in parenthesis wre obtained and treated in the same manner as in the previous section. The magnitudes of dimensionless terms of inertia (e.g., $\tilde{v}_r(\partial\tilde{v}_r/\partial\tilde{r})$ are the same order as those of pressure (i.e., $-\partial\tilde{P}/\partial\tilde{r}$) and viscosity (i.e., $\partial^2\tilde{v}_r/\partial\tilde{z}^2$) except for the cases of right-hand-side fan-shaped cavities as in Figs. 12(a)-(c), where those of dimensionless terms of inertia (e.g., $\tilde{v}_r(\partial\tilde{v}_r/\partial\tilde{r})$ are 15 times larger than those of pressure (i.e., $-\partial\tilde{P}/\partial\tilde{r}$) and viscosity (i.e., $\partial^2\tilde{v}_r/\partial\tilde{z}^2$). Even for these cases, however, neglecting the inertia term may be valid even at $r=R_1$ since the magnitudes of $\rho\bar{v}_r H\mu/(H/R_0)$ are so small as to be the order of 10^{-4} to 10^{-5}.

Since the vertex angle of left fan was twice as much as that of the fan on right hand side as in Figs. 11(a) to 11(c), the edge effect of the left fan would be smaller than that of the right fan, while the edge effect would not have to be considered in Figs. 12(a) to 12(c) where the vertex angles of both fans were the same. Even though this edge effect was not remarkable when the length of R_0 on both sides of fans was the same as in the previous article of 1) Results with the same length of initial polymer shut offs, this effect of the right fan might be doubled due to its doubled length of R_0 as in Figs. 11(a) to 11(c) (with different vertex angles of both fans) where the values of SR were much less than those of the ratios of resistances in Table 7, unlike the cases of Figs. 9(a) to 9(c) (with the same vertex angles of both fans) from Table 6. In particular, the discrepancies between SR and the ratio of resistances (i.e., discrepancy=|SR-Ratio of resistance/SR|) from Table 7 were amplified in case of Figs.

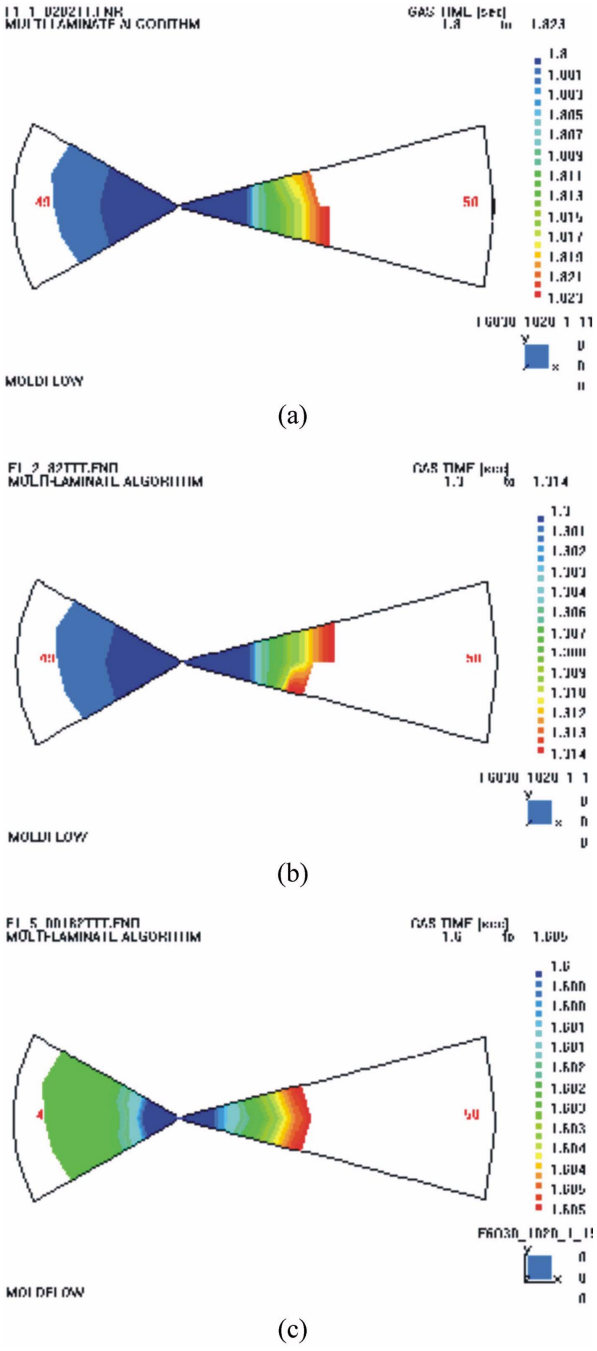

Fig. 11. Simulated gas penetration: (a) Left: $\hat{\theta}$=60°, R_0=10 mm, H=1 mm; Right: $\hat{\theta}$=30°, R_0=20 mm, H=1.1 mm; (b) Left: $\hat{\theta}$=60°, R_0=10 mm, H=1 mm; Right: $\hat{\theta}$=30°, R_0=20 mm, H=1.2 mm; (c) Left: $\hat{\theta}$=60°, R_0=10 mm, H=1 mm; Right: $\hat{\theta}$= 30°, R_0=20 mm, H=1.5 mm.

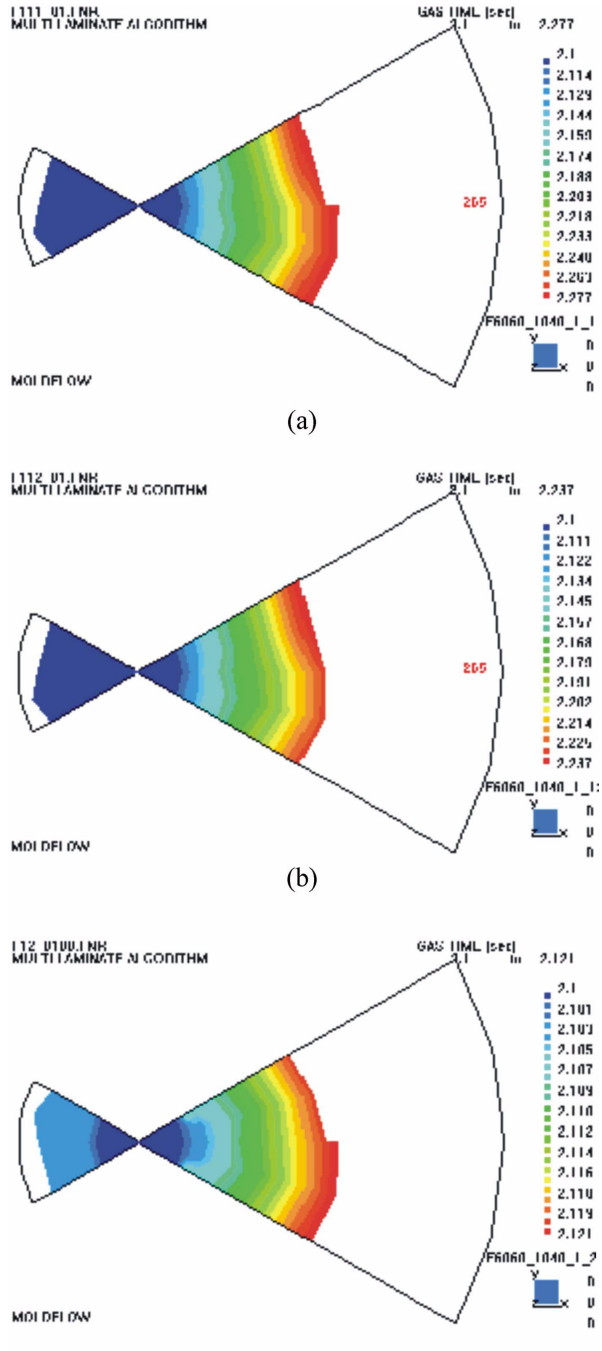

Fig. 12. Simulated gas penetration: (a) Left: $\hat{\theta}$=60°, R_0=10 mm, H=1 mm; Right: $\hat{\theta}$=60°, R_0=40 mm, H=1.1 mm; (b) Left: $\hat{\theta}$=60°, R_0=10 mm, H=1 mm; Right: $\hat{\theta}$=60°, R_0=40 mm, H=1.2 mm; (c) Left: $\hat{\theta}$=60°, R_0=10 mm, H=1 mm; Right: $\hat{\theta}$= 60°, R_0=40 mm, H=2 mm.

11(a) and 11(b) because the ratios (left/right) of the values of H/R_0 on left and right sides from Figs. 11(a) and 11(b) became bigger than that from Fig. 11(c) by the same reasoning as in the previous section. In the same manner, in case of Figs. 12(a) to 12(c), the discrepancy between SR and the ratio of resistance was observed to increase as in Table 7 as the ratio (left/right) of the values of H/R_0 on left and right sides became bigger. Nonetheless, it was confirmed again that the direction of gas flow was always correct so that the rule of thumb of Eq. (19) might be still effective when the definition of direction of gas flow is used as previously defined.

The discrepancy that occurred between the ratio of SR and the suggested ratio of resistances (Eq. (19)) was believed to result generally from two assumptions made in the rule of thumb.

1. Since the purpose of this paper was to qualitatively diagnose

the instantaneous gas flow direction under fan-shaped geometry, it was assumed acceptable to treat a non-Newtonian fluid as a Newtonian fluid.

2. Coated layer was assumed neglected in the mass balance equation by which the suggested rule of thumb (Eq. (19)) was derived.

One may consider the coated layer (i.e., frozen layer and hydrodynamic layer) left behind when gas pushes the resin to flow forward. As gas pushes the resin further, the hydrodynamic resistance between resin-flow and mold walls becomes smaller because the coated layer left behind the resin flow accumulates on the surface of mold and the remaining mass of resin flow becomes less. Due to the accumulated coated layer on the surface of mold, the resin velocity to the direction of gas flow becomes accelerated, which shall be treated in part 2 of the paper. Due to the acceleration of gas flow, the shear-rate thinning property of pseudo-plastic fluid of melt resin accelerates the gas flow in return more than Newtonian fluid property does. In addition, since volume control was adopted instead of pressure control as gas control in simulation, the pressure was supposed to decay so that the velocity of gas flow might become less once the accelerated melt front of resin was blocked against the mold-barrier of one direction and the direction of gas flow was reversed to the other direction. Thus, the gas generally determines the flow to the direction of least resistance of the initial stage. The initial period of interest for gas to penetrate and push forward the static melt fluid and to determine the direction is such a transient period that the strategy employing Newtonian viscosity may not be too crude an assumption to predict, not quantitatively but qualitatively, the direction of gas path in GAIM, which is supposed to be the direction of least resistance. Further, the gas direction determined by the suggested rule of thumb would not generally deviate from that in reality, even though the accumulated mass of coated layer was not considered in the rule of thumb, since, in reality, the velocity of resin became accelerated in GAIM to the direction determined due to the diminishing resistance of melt resin against mold wall. Therefore, the rule of thumb suggested with the assumption to neglect the coated layer was qualitatively valid as far as the gas direction was concerned.

CONCLUSIONS

The results of simulation (SR) were compared with the ratios of resistances as well as the predicted direction of the gas flow in GAIM by using the rule of thumb suggested upon performing the simulation with commercial software (MOLDFLOW). The simulation and the prediction by the suggested rule of thumb were performed in three categories: 1) the cases with the same lengths of initial polymer shut-offs; 2) the cases with the same vertex angle of fan shapes; and 3) the case with various vertex angles of fan shapes, various lengths of initial polymer shut-offs and various thickness of cavities.

The predictions by the suggested rule of thumb were quite well matched by the simulation-results of MOLDFLOW. However, the discrepancy between SR and the ratio of resistances was observed to increase as the ratio $\left(\frac{\text{more}(H/R_0)(\text{one-side})}{\text{less}(H/R_0)(\text{the other-side})}\right)$ of the values of H/R_0 on both sides of fan-shaped cavities became bigger. Nevertheless, the suggested rule of thumb was still effective as far as the direction of gas flow was concerned.

The discrepancy occurred between SR and the suggested ratio of resistances was believed to result generally from the assumption of Newtonian fluid as well as that of no coated layer accumulated at the wall of mold. However, the strategy employing Newtonian viscosity may not be too crude an assumption to predict, not quantitatively but qualitatively, the direction of gas path in GAIM. Further, the gas direction determined by the suggested rule of thumb would not generally deviate from that in reality even though the accumulated mass of coated layer was neglected in the rule of thumb.

ACKNOWLEDGMENT

This research was supported (in part) by the Daegu University Research Grant, 2002.

NOMENCLATURE

- h : distance between top or bottom plate and centerline of the cavity
- H : distance between two parallel plates
- P : pressure
- P_1 : pressure at $r=R_1$
- P' : pressure at $r=R'$
- P_0 : pressure at $r=R_0$
- $\overline{P}$: characteristic pressure
- Q : flow rate of melt resin
- R_1 : radius of nozzle for melt resin- or gas-injection
- R_0 : radius of initial polymer shut off
- R' : position randomly chosen in r direction between $r=R_1$ and $r=R_0$
- r : coordinate in cylindrical coordinate
- $\tilde{r}$: dimensinless radial coordinate
- $r^{\#}$: resistance to Q
- r^{*} : resistance to V^{*}
- SR : ratio of simulated gas penetration lengths to both of right and left directions until either right and left leading fronts of melt polymer reaches mold barrier first
- $\hat{t}$: characteristic time
- $\tilde{t}$: dimensionless time
- V^{*} : initial velocity of melt polymer at the nearest geometry to a gas injection point
- V_r : velocity in r direction
- V_z : velocity in z direction
- $\overline{V}_r$: characteristic velocity in r direction
- $\overline{V}_z$: characteristic velocity in z direction
- $\tilde{V}_r$: dimensionless radial velocity
- $\tilde{V}_z$: dimensionless axial velocity
- $\langle V_r \rangle$: average radial velocity
- z : coordinate in cylindrical coordinate
- $\tilde{z}$: dimensinless axial coordinate

Greek Letters

- ρ : density of polymer melt phase
- θ : coordinate in cylindrical coordinate
- $\hat{\theta}$: vertex angle of the fan-shaped radial flow

$\tilde{\theta}$: dimensionless θ coordinate
μ : Newtonian viscosity

REFERENCES

Chen, S.-C., Cheng, Hsu, K.-F. and Hsu, K.-S., "Polymer Melt Flow and Gas Penetration in Gas Assisted Molding of a Thin Part with Gas Channel Design," *Int. J. Heat Mass Transfer*, **39**, 2957 (1996b).

Chen, S.-C., Cheng, N.-T. and Chao, S.-M., "Simulations and Verification of Melt Flow and Secondary Gas Penetration During a Gas Assisted Injection Molding," *International Polymer Processing*, **14**, 90 (1998).

Chen, S.-C., Cheng, N.-T. and Hsu, K.-S., "Simulations and Verification of the Secondary Gas Penetration in a Gas Assisted Injection Molded Spiral Tube," *International Communications in Heat and Mass Transfer*, **22**, 319 (1995).

Chen, S.-C., Cheng, N.-T. and Hsu, K.-S., "Simulations of Gas Penetration in Thin Plates Designed with a Semicircular Gas Channel During Gas Assisted Injection Molding," *Int. J. Mech. Sci*., **38**, 335 (1996a).

Gao, D. M., Nguyen, K. T., Garcia-Rejon, and Salloum, G., "Optimization of the Gas Assisted Injection Moulding Process Using Multiple Gas-injection Systems," *Journal of Materials Processing Technology*, **69**, 282 (1997).

Kennedy, P., "Flow Analysis of iNjection Molding," Hanser Publishers, Munich Vienna New York (1995).

Khayat, R. E., Derdouri, A. and Herbert, L. P., " A Three-dimensional Boundary-element Approach to Gas Assisted Injection Molding," *J. Non-Newtonian Fluid Mech*., **57**, 253 (1995).

Lim, K. H. and Lee, E. J., "Prediction of Gas Flow Directions in Gas Assisted Injection Molding when Cavities and Runners are Involved," *Korean J. Chem. Eng*., **20**(3), 592 (2003).

McCabe, W. L., Smith, J. C. and Harriot, P., "Unit Operations of Chemical Engineering," 4th Ed., McGraw-Hill Press (1986).

Parez, M. A., Ong, N. S., Lam, Y. C. and Tor, S. B., "Gas-assisted Injection Molding: the Effects of Process Variables and Gas Channel Geometry," *Journal of Material Processing Technology*, **121**, 27 (2002).

Patankar, S. V., "Numerical Heat Transfer and Fluid Flow," McGraw-Hill Book Company, New York (1984).

Shen, Y. K., "Study on Polymer Melt Front, Gas Front and Solid Layer in Filling Stage of Gas Assisted Injection Molding," *Int. Comm. Heat Mass Transfer*, **28**, 139 (2001).

Shen, Y. K., "Study on the Gas-liquid Interface and Polymer Melt Front in Gas Assisted Injection Molding," *Int. Comm. Heat Mass Transfer.*, **24**, 295 (1997).

Soh, Y. S. and Lim, K. H., "Control of Gas Direction in Gas Assisted Injection Molding; Definition of Resistance to Velocity, $r_{\bar{v}}$," SPE ANTEC Tec. Papers, **60**, 482 (2002).